Published in Material Science and Engineering A, 2003, Vol 346, Iss 1-2

Optimization of mechanical properties of an HSLA-100 steel through control of heat treatment variables

P.K. Ray [a,*], R.I. Ganguly [b], A.K. Panda [b]

[a] *Department of Applied Mechanics and Hydraulics, Regional Engineering College, Rourkela 769 008, India*
[b] *Department of Metallurgical Engineering, Regional Engineering College, Rourkela 769 008, India*

Abstract

HSLA-100 steel is widely used in Navy vessels, where the requirement is a steel with good weldability possessing a high strength together with a high degree of low-temperature toughness property. However, an increase in strength is usually accompanied by a decrease in toughness. Hence there is a need for optimization of the properties. The present work attempts to optimize the mechanical properties of an HSLA-100 steel through control of heat treatment process parameters. Initially single factor experiments are carried out over a wide range of tempering time–temperature combinations to identify the heat treatment zone where the optimum combination of properties is likely to be obtained. Further experiments are done in this zone through statistical design of experiments. The present work involves quantification of properties by: (i) classical curve fitting technique with data obtained from single factor experiments; and (ii) forming regression equations from 2^2 factorial design of experiments. Subsequently maximization of low-temperature impact property has been done within the experimental region by Steepest Ascent method, and finally optimum combination of the properties of the present steel has been obtained by Grid Search technique with a constraint on yield strength. Transmission Electron Microscopy studies are made with a view to understanding and correlating the mechanical properties with the microstructures.

Keywords: HSLA steel; Heat treatment; Optimization; Design of experiments; Mechanical properties

1. Introduction

HSLA-100 steel is designed for yield strength ≥ 100 ksi (~ 700 MPa) and impact strength ≥ 81 J at -84 °C [1,2]. The alloy chemistry of this steel makes it responsive to heat treatment and thermomechanical processing [3]. Since the steel has a very low carbon content (≤ 0.06 wt.%) to improve weldability, other alloying elements are added to increase strength and impact properties. While Mo, Cr, Ni increase hardenability, Cu in the steel increases strength through formation of fine precipitates of copper during tempering [4] and increases weathering resistance. It also lowers the martensite/bainite transformation temperature and retards recovery and recrystallization of as-quenched steel [5,6]. Addition of Nb in micro level makes the steel HSLA grade and amenable to thermomechanical processing [7].

The steel used in the present study finds application in navy vessels, which calls for high strength along with a high value of low-temperature impact property [8]. There exists a number of ways of strengthening steel, viz. precipitation hardening, martensitic/bainitic hardening, solid solution hardening, grain refinement. However, while the strength increases, there is a corresponding decrease in impact property. Hence there is a need to define the processing variables for an optimum combination of strength and toughness.

Literatures [5,6,9] show that there have been attempts to maximize/optimize properties by single variable technique, i.e. varying one variable at a time keeping the other variables constant. However, this technique does not take into account the complex interaction effects of the variables, i.e. the combined effect on the response (dependent variable) when the process para-

meters (independent variables) change simultaneously. The present study attempts to quantify the mechanical properties (responses) with respect to heat treatment parameters (process variables) by classical curve fitting technique and then applying statistical design of experiments, where the independent variables are altered simultaneously in a planned schedule. Because of the complex nature of the equations derived by classical curve fitting technique, it is difficult to perceive and visualize the response surfaces. Hence, use is made of 3-D plots to conceive the variation of the response (i.e. property in one axis) with the process variables (i.e. heat treatment parameters in the other two axes). Finally maximization of strength properties has been done using Steepest Ascent method while optimization has been done by Grid Search technique. Attempt has also been made to correlate microstructure with the mechanical properties obtained after each heat treatment schedule.

2. Optimization/maximization techniques

Optimization is a tool for obtaining the best possible combination of effects under a given set of circumstances (constraints), either to maximize the desired benefits or to minimize the resources. The classical method of differential calculus to obtain maxima/minima of an unconstrained function assumes that the function is continuous and differentiable twice. Hence, various other techniques of optimization have been evolved [10,11]. The following describes in brief the techniques used in the present study.

2.1. Classical curve fitting technique

In this method single factor experiments are carried out to generate data. These data are fitted to suitable equations by least-square fit method. Usually a number of different forms of equations is tried and the one which gives the regression coefficient (R^2) nearly equal to unity with minimum standard error of estimate is considered to be the best fit. The equations so formed are valid within the range of experimental variables. For a function involving three variables, 3-D graphs can be plotted, from which it is possible to understand the nature of the variation of the dependent variable (response).

2.2. Statistical design of experiments

In factorial design of experiments the effects of different factors are investigated by simultaneously varying the factors [12–15]. For the purpose of optimization using single factor experiment, a factor (say A) is varied while the levels of the other factors (say B, C, D) are fixed before the start of the experiment. Usually the levels of the other factors are decided based on prior information. The experiment reveals the effects of A, for a particular combination of the factors B, C, D. However, in such case obtaining an optimum solution is a chance process since the variable A may interact differently at different levels of other factors (B, C, D) owing to complex interactions occurring due to different strengthening/softening mechanisms involved at various levels.

Under such circumstances, the factorial design of experiments is judiciously planned where all the factors are simultaneously changed from a base level value. Usually these levels are decided from prior information obtained either from literature or from single factor experiments. Thus a design matrix is formed covering a region of small variation of the factors. The response surface so obtained is more or less plane in nature. Since the variables are changed simultaneously, the method gives the quantitative effect of interaction of the variables on the properties. Nomograms (i.e. isoproperty lines) may be constructed, which may fruitfully be used to decide on the process parameters for desired properties.

2.3. Method of steepest ascent

This is one of the available methods of non-linear multivariable programming without constraints. Thus it is primarily a maximization method. The method of maximizing using single factor experiment is by trial and error and hence time consuming. Further it becomes complicated when the number of variables increases. In such cases various optimization/maximization tools, such as Steepest Ascent method [10,11], are found to be useful. The *method of steepest ascent* is a process of maximization following the steepest path which is the gradient vector of the function to be maximized. By following the reverse direction of the slope (path) the minima of a function can be obtained and in that case the process is known as the *method of steepest descent*.

The partial derivatives of a function $\Phi(x)$, with respect to each of the n variables $x_1, x_2, \ldots, x_n$, are collectively called the gradient of the function and is denoted by,

$$\nabla\Phi(x) = \boldsymbol{X}_i = \begin{matrix} \partial f/\partial x_1 \\ \partial f/\partial x_2 \\ \vdots \\ \partial f/\partial x_n \end{matrix}$$

The gradient vector has a unique property of possessing the steepest slope, i.e. its direction is normal to the curve at a point on $\Phi(x)$ in an n-dimensional space, thus providing the shortest path to the optima.

The contour of $\Phi(x)$ changes with change in the values of $x_1, x_2, \ldots, x_n$. Hence, the direction of the normal also changes. Thus it is necessary to obtain the

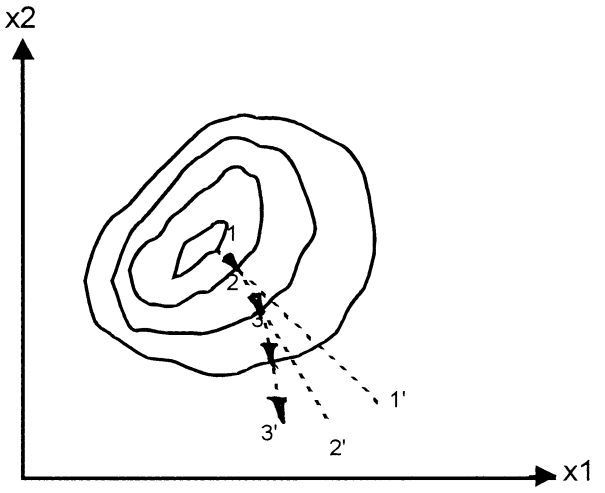

Fig. 1. Steepest ascent directions.

normal and refix the path direction in incremental steps. This is explained in Fig. 1.

The initial gradient vector $\boldsymbol{X}_1$, i.e. the starting point, is chosen making use of any prior information about where the desired global maxima could be found. The vectors $\boldsymbol{X}_1$, $\boldsymbol{X}_2$, $\boldsymbol{X}_3$, ... are found by iterative relation. The iterative process terminates if and when the difference between the values of the objective function at two successive $\boldsymbol{X}$-vectors is smaller than a prescribed tolerance.

2.4. Grid search technique

This is a multivariable non-linear optimization technique with constraints $\boldsymbol{X}_i$. The basic idea is to divide the field into k number of segments (i.e. $k+1$ nodes in each of the variables). Function values are computed at each of the $(k+1)^n$ nodes, where n is the number of variables. The largest value and the corresponding value of $\boldsymbol{X}_i$ are stored after comparing with the function value at each node. However, at any particular point if any one of the constraints is violated, that point is discarded in the calculation. For a finite field and less number of variables this method is very effective since it gives an idea of the entire field and yields a global maximum. If required any further refinement can be carried out around the maximum point obtained. A suitable computer program can be prepared and used for this search technique [10,11].

3. Experimental

The steel, designated GPP, was received from the U.S. Naval Research Laboratory. The chemical composition of the steel is given in Table 1. The steel was examined for inclusion content. The grain sizes were measured using Quantimet-570 image analysis system.

Initially heat treatment was carried out at three different austenitization temperatures (900, 950, 1000 °C) followed by quenching in water, and then tempering at temperatures ranging from 450 to 700 °C at intervals of 50 °C. As reported elsewhere [5,6,9,16], a zone was defined between 600 and 700 °C tempering temperature where the strength property increases and also the Charpy impact value is high. Therefore, further experiments were carried out by tempering the steel in this temperature range for different lengths of time.

The material was received in the form of plate having dimension $250 \times 300 \times 50$ mm^3 thick. All the samples for tensile and low-temperature (−50 °C) Charpy impact tests were prepared from the mid-40 mm thickness of the plate in L–T orientation. The tensile tests were done in an Instron-1195 machine as per ASTM E-8-78 methodology at a crosshead speed of 5 mm min^{-1}. All the Charpy impact tests were done at −50 °C. The fractured surfaces of broken Charpy samples were examined in a JEOL Scanning Electron Microscope.

For transmission electron microscopy (TEM) thin specimens (0.5 mm) were cut from the broken Charpy test samples in an Isomet machine. Further thinning was done in alternate steps of chemical thinning and mechanical thinning till the specimen thickness was reduced to 0.3 mm. Chemical thinning was done using a solution of 40% Nitric acid, 10% Hydrofluoric acid and 50% water. Finally discs of 3 mm diameter were punched out and were further thinned electrolytically in a Fischione twin-jet elctro-polisher using a solution of 33% Perchloric acid and 67% Ethanol. The solution bath was kept cool by liquid nitrogen. These thin foils were then examined in a JEOL TEM at an operating voltage of 100 kV.

Table 1
Chemical composition of the steel

Element	Composition (wt.%)
C	0.04
Mn	0.86
P	0.004
S	0.002
Si	0.27
Cu	1.58
Ni	3.55
Cr	0.57
Mo	0.60
Al	0.032
Cb	0.030

4. Results and discussions

The chemical composition of the steel is given in Table 1. The steel was examined for inclusion content which was found to be very low ($< 10^{-4}$ area fraction). The average grain size was about 7–8 μm. The mechanical properties of the steel in as-received condition are given in Table 2.

It is observed from the tempering temperature vs. hardness curves (Fig. 2) that there is an increase in the hardness value in the vicinity of tempering temperature of 450 °C, after which there is a sharp decrease in hardness value with increasing tempering temperature up to 600 °C, whereupon the hardness again increases between 640 and 700 °C.

TEM studies reveal lath structure with coherent Cu-rich clusters at a tempering temperature of 450 °C (Fig. 3). The blurred regions indicate coherency strains due to the Cu precipitates. The increase in strength and hardness at this temperature is due to the precipitation of fine coherent Cu-precipitates along with dislocations and coherency strains in the lath martensite without any recovery [5,6].

Tempering at 600 °C shows partial recovery and clean ferrite is seen with a few precipitates (Fig. 4). The matrix appears to have recovered without recrystallization. The decrease in hardness at this tempering temperature is due to the coarsening of the precipitates with recovery in the matrix. No attempt was made to analyze the dark precipitates observed in the microstructure.

Tempering at 700 °C shows formation of new generation austenite at the prior lath boundary, which are parallel to the lath (Fig. 5). It is reported by Mujahid et al. [5,6] that in the early stages of formation, the new austenite is rich in solutes such as Ni, Cu, Mn and Cr. This austenite is highly stable because of the presence of austenite stabilizing agents like Ni and Cu [5,6] and is retained on cooling. However, at higher tempering temperature the growth of the austenite causes a dilution in the volume fraction of the stabilizing agents and the newly formed austenite changes to martensite/bainite structure on quenching. This is why the hardness increases and there is a second peak in the hardness curve (Fig. 2) in the higher tempering temperature range. The new austenite also causes an improvement in the toughness of the steel [5,6].

Table 2
Mechanical Properties of the as-received material

	Supplied[a]	Experimental
YS (MPa)	772.9	746.2
TS (MPa)	830.2	804.8
YS/TS	0.93	0.93
%EL on 25 mm GL	24	28

[a] Value supplied by the U.S. agency.

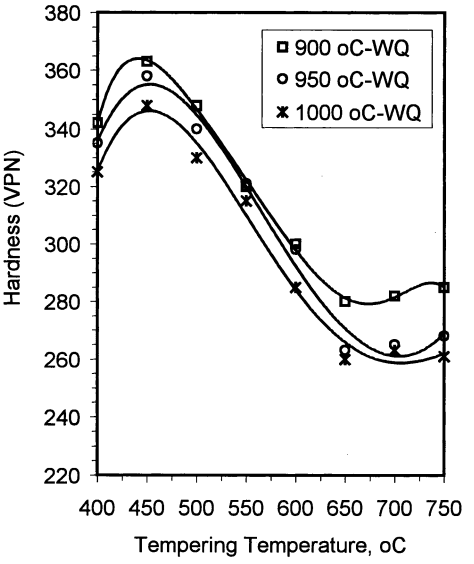

Fig. 2. Tempering temperature vs. hardness curves.

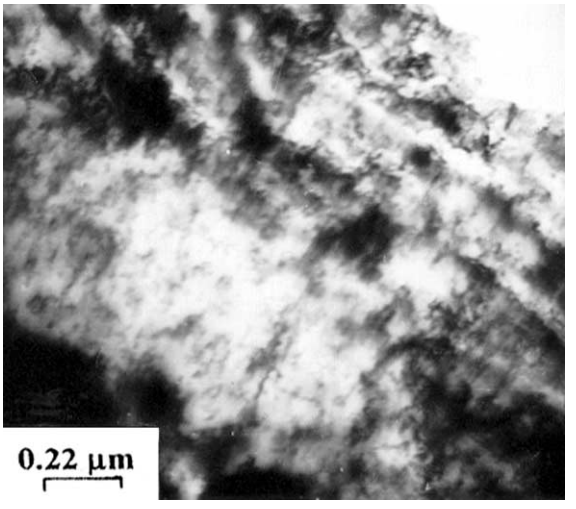

Fig. 3. TEM of steel tempered at 450 °C (1 h). The blurred regions indicate coherency strains due to Cu precipitates during the early stages of tempering.

The scanning electron micrograph (SEM) of the fracture surface of broken Charpy sample tempered at 450 °C (Fig. 6) shows quasi-cleavage nature (typical brittle fracture), while the same for sample tempered at 700 °C (Fig. 7) shows dimples on the fracture surface (a characteristic of typical ductile fracture).

The tensile tests carried out on steel tempered at 600 °C show discontinuous yielding (Fig. 8) with a high value of yield strength to tensile strength (YS/TS) ratio (~ 0.98) indicating less work hardening. This may be attributed to the recovery (Fig. 5) of the matrix from quenched-in stresses [4]. The transmission electron micrographs of specimens tempered at 600 °C (Fig. 4)

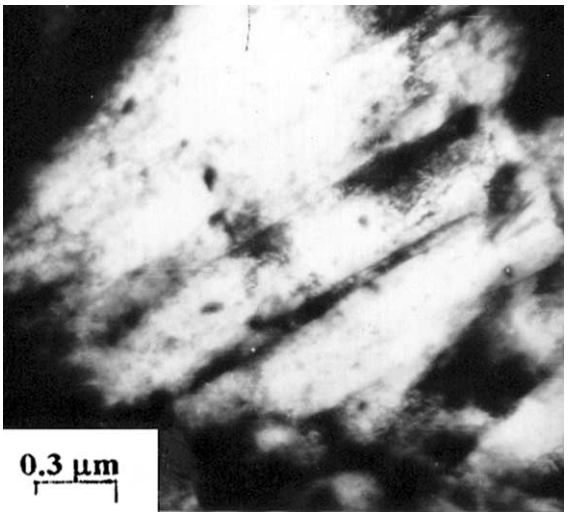

Fig. 4. TEM of steel tempered at 600 °C (1 h) shows occurrence of recovery in the lath structure with distinct precipitates in the matrix.

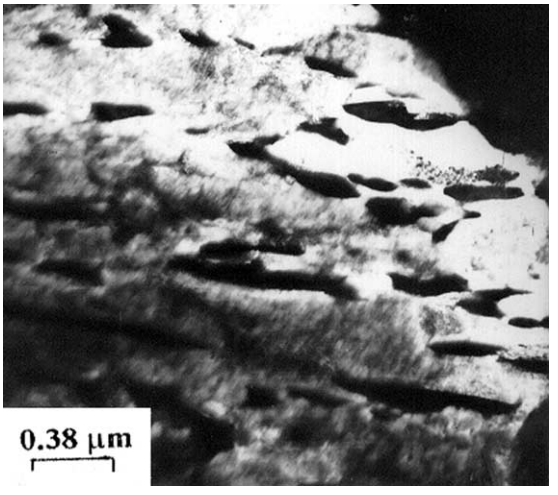

Fig. 5. TEM of steel tempered at 700 °C (1 h) shows new generation austenite at prior lath boundaries.

shows a recovered structure (ferrite with a few precipitates). However, for the specimens tempered at 700 °C there is formation of new generation austenite which transformed to martensite/bainite on quenching, and thus represents a dual phase structure. The stress–strain curve for specimens tempered at 700 °C show continuous yielding (Fig. 8) with YS/TS ratio varying between 0.64 and 0.88 (Table 3). This is a typical characteristic of a dual phase steel. The same conclusion can also be reached from the plots of YS and TS vs. Hollomon–Jaffe temperature normalized time parameter. It is seen from Fig. 9 that the YS values at all tempering temperatures bear a linear dependence on this parameter. However, the TS values deviate significantly from linearity at higher tempering temperatures (Fig. 10). Foley and Fine [9] explained this deviation of TS at higher tempering temperatures due to the formation of

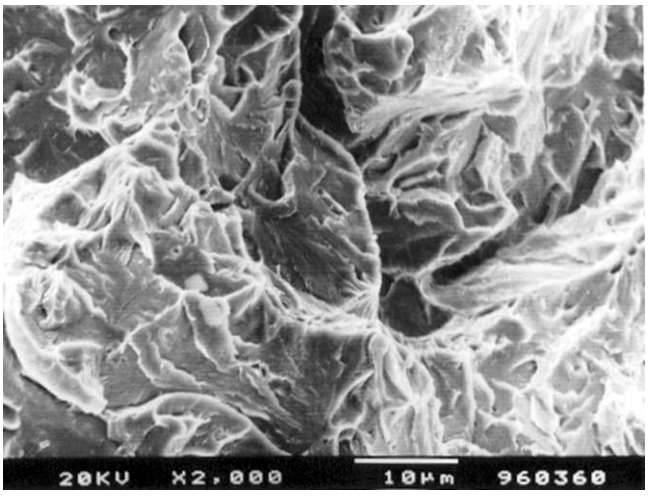

Fig. 6. SEM fractograph of broken Charpy sample tempered at 450 °C (1 h) shows quasi-cleavage fracture (test temperature = −50 °C).

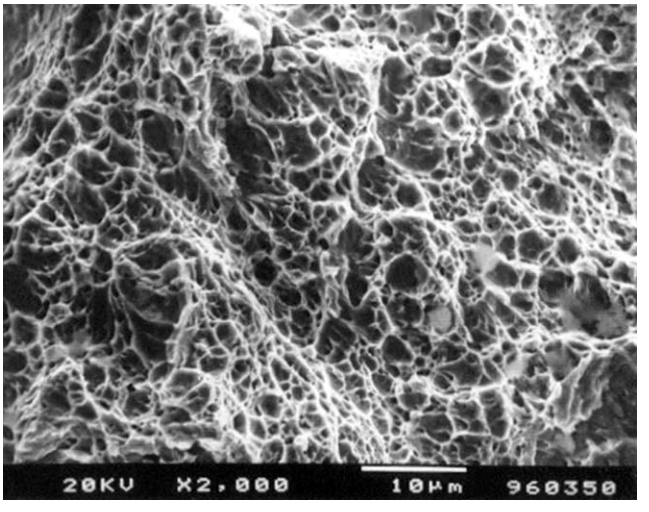

Fig. 7. SEM fractograph of broken Charpy sample tempered at 700°C (1 h) shows dimples on the fracture surface (test temperature = −50 °C).

new austenite at higher tempering temperatures as explained earlier.

It was therefore decided to carry out a detailed investigation in this region of tempering temperature, i.e. 600–700 °C where both strength and toughness improve [5,6,9,16]. For this purpose the steel was tempered at 600 and 700 °C for different lengths of time. The results of the tensile tests of such specimens are shown in Table 3.

Using least-square curve fitting technique the following equations for YS and TS are derived from the data of Table 3.

$$\text{YS (MPa)} = (1702.03 - 1.55T)t^{(2.8107 - 0.4496 \ln T)}, \quad (1)$$

$$\text{TS (MPa)} = (876.03 - 0.14077T)t^{(0.4153 - 0.075 \ln T)}, \quad (2)$$

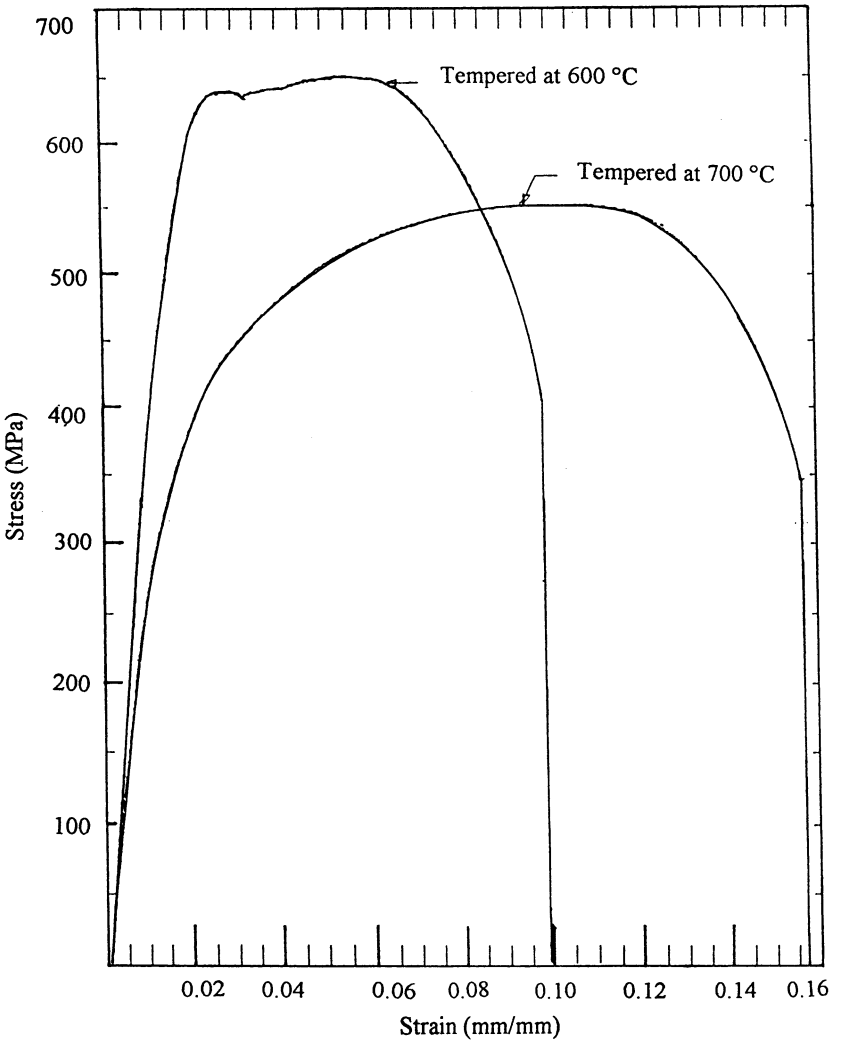

Fig. 8. Typical stress–strain diagram of steel tempered at 600 and 700 °C.

Table 3
Tensile properties of the steel after tempering at different combinations of temperature and time

Tempering temperature (°C)–time (h)	YS (MPa)	TS (MPa)	YS/TS	*n*
700–0.33	733.8	831.9	0.88	0.20
700–2	544.5	750.5	0.73	0.21
700–12	436.5	652.4	0.67	0.24
700–80	348.3	543.5	0.64	0.20
600–0.33	846.6	863.3	0.98	0.069
600–2	716.1	735.8	0.97	0.12
600–12	670.0	680.8	0.98	0.13
AQ	861.3	943.7	0.91	–

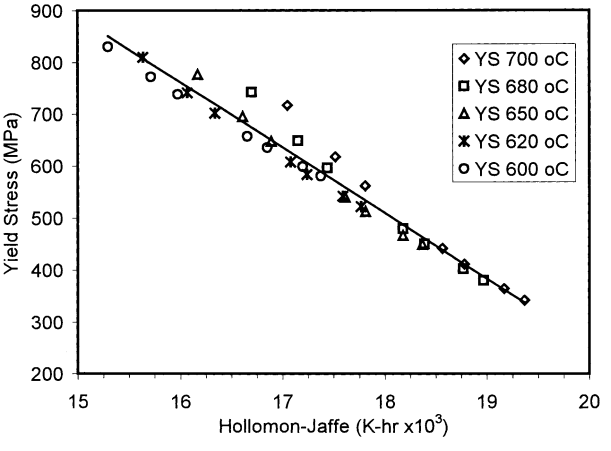

Fig. 9. Yield stress vs. Hollomon–Jaffe parameter.

where T is the tempering temperature in °C and t is the tempering time in hours.

Fig. 11 shows variation of ratio of YS/TS, calculated using Eqs. (1) and (2), with tempering time for different values of tempering temperature. It can be seen from the plot that below a tempering temperature of 615 °C the ratio of YS/TS remains fairly constant for all values of tempering time. The variation of the ratio of YS/TS

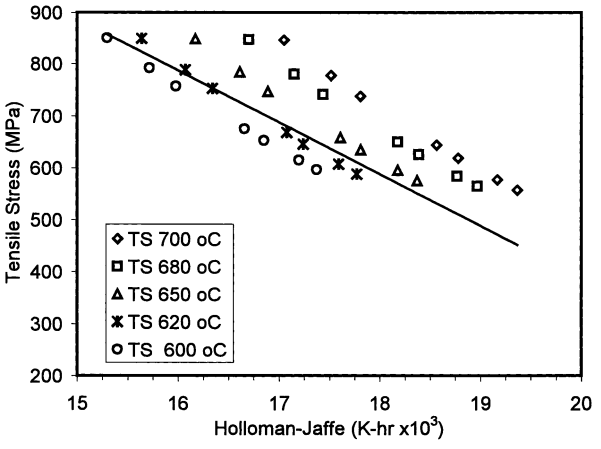

Fig. 10. Tensile stress vs. Hollomon–Jaffe parameter.

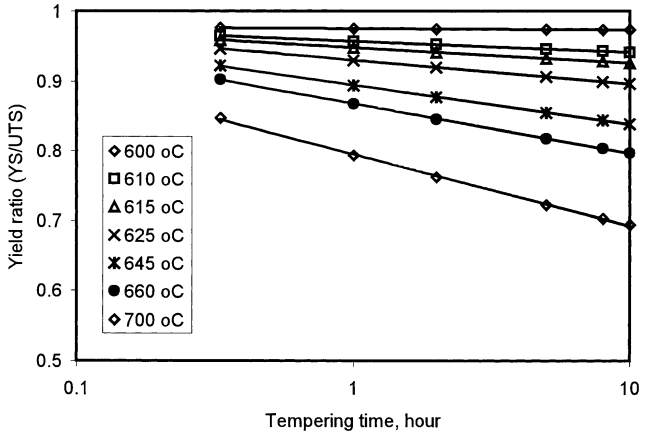

Fig. 11. Variation of YS/TS with tempering time.

becomes significant at a temperature of 645 °C indicating the onset of new austenite formation and a continuous stress–strain curve. The Ac_1 temperature for this steel was experimentally obtained as 660 °C [16]. Thus the regression equations give an estimate of the temperature at which the ratio of YS to TS begins to vary with tempering time due to the formation of dual phase structure.

Table 4
−50 °C CVN energy values of the steel at different combinations of tempering temperature and time

Tempering temperature (°C)–time (h)	−50 °C CVN energy (J)
700–0.33	258
700–1.0	235
700–2.0	232
700–12	180
700–80	208
600–0.33	135
600–1.0	176
600–2.0	196
600–12	215

Table 4 shows the −50 °C Charpy impact values obtained under different heat treatment conditions. Eq. (3), given hereunder, has been obtained by least-square curve fitting method using the data of Table 4.

$$\begin{aligned}\text{Charpy value (J)} &= (0.030219T - 21.0747)\,t^2 \\ &\quad + (0.494753T + 339.5288)t \\ &\quad + (1.2221T - 606.6),\end{aligned} \tag{3}$$

where T is the tempering temperature in °C and t is the tempering time in hours.

The Eqs. (1)–(3) are valid within tempering time range of 0.33–12 h and tempering temperature range of 600–700 °C. Fig. 12 shows the 3-D plot of −50 °C CVN value superimposed on YS. Fig. 13 shows the superimposed contour plots of YS and Charpy value. The following observations can be made from these plots. The optima (i.e. where both YS and CVN values are high) lies in the vicinity of tempering time of 0.5 h and tempering temperature of 680 °C as evident from Figs. 12 and 13.

Using the above as the prior information, experiments are planned with tempering time varying between 0.33 and 2 h (base level = 1.665 h) and tempering temperature varying between 600 and 700 °C (base level = 650 °C). The 2^2 design matrix with the responses is shown in Table 5, and the regression equations developed are:

$$\begin{aligned}\text{YS (MPa)} &= 710.24 - 71.10X_1 - 79.95X_2 \\ &\quad - 14.70X_1X_2,\end{aligned} \tag{4}$$

$$\begin{aligned}Y_{\text{charpy}}\text{(J)} &= 205.25 + 39.75X_1 + 8.75X_2 \\ &\quad - 21.75X_1X_2,\end{aligned} \tag{5}$$

where

$$\begin{aligned}X_1 &= (x_1 - 650\ ^\circ\text{C})/50, \\ X_2 &= (x_2 - 1.165\ \text{h})/0.835,\end{aligned} \tag{6}$$

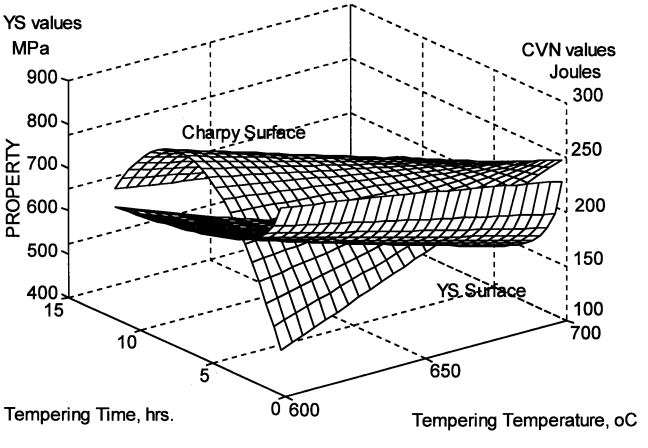

Fig. 12. Yield strength response surface superimposed on −50 °C Charpy response surface (region: 600–700 °C and 0.33–12 h).

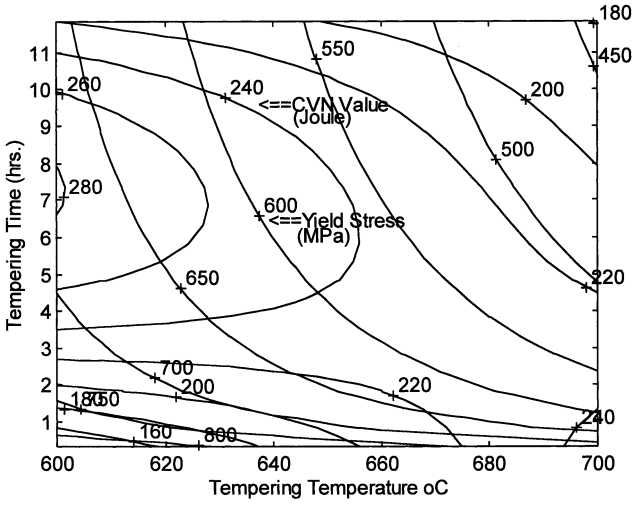

Fig. 13. Superimposed contour plot of YS and −50 °C CVN value (region: 600–700 °C and 0.33–12 h).

x_1 and x_2 are natural values of temperature (in °C) and time (in hours) of tempering. Y_{charpy} is the Charpy impact value at −50 °C in Joule. X_1 and X_2 are the coded values of tempering temperature and time, respectively. The range of variation of both X_1 and X_2 is −1 to +1 corresponding to the minimum and maximum values of temperature and time as will be evident from Eq. (6). The coded values are to be inserted in the Eqs. (4) and (5) to obtain the values of YS and Y_{charpy}, respectively. The natural values of temperature and time of tempering (i.e. x_1, x_2) can be obtained by decoding the coded values (i.e. X_1, X_2) using Eq. (6).

The negative coefficient of X_1 in Eq. (4) indicates a decrease in YS for an increase in tempering temperature above the base level (650 °C⇒positive X_1). However, this decrease in YS is partly compensated if the tempering time is kept below the base level value (1.165 h⇒negative X_2) since the coefficient attached to X_2 is negative. Further the temperature–time interaction coefficient (i.e. the coefficient of X_1X_2) being negative, the positive X_1 and negative X_2 combination helps in increasing the YS. Under these conditions, the positive coefficient of X_1 in Eq. (5) suggests that there is an increase in Charpy value for tempering temperature above the base level (650 °C⇒positive X_1). The positive coefficient of X_2 in Eq. (5) suggests that there will be loss in Charpy value for tempering time below the base level value (1.165 h⇒negative X_2). However, this decrease is not much since the numerical value of the coefficient is small. Further negative interaction coefficient means that there will be increase in net Charpy value with positive X_1 and negative X_2. Thus the gain in Charpy value will be more for a little sacrifice in YS if the tempering temperature is increased above the base level. Hence it is concluded that the optimum combination of properties will prevail at a tempering temperature above the base level value (i.e. >650 °C⇒positive X_1) and a tempering time below the base level value (i.e. <1.165 h⇒negative X_2).

Figs. 14 and 15 show 3-D plots of YS and Charpy value against the coded values of temperature (X_1) and time (X_2) of tempering. Since the range of tempering time has now been narrowed down to 0.33–2 h, the complex topology of the response surfaces (Fig. 12) can now be approximated to a plane surface (Figs. 14 and

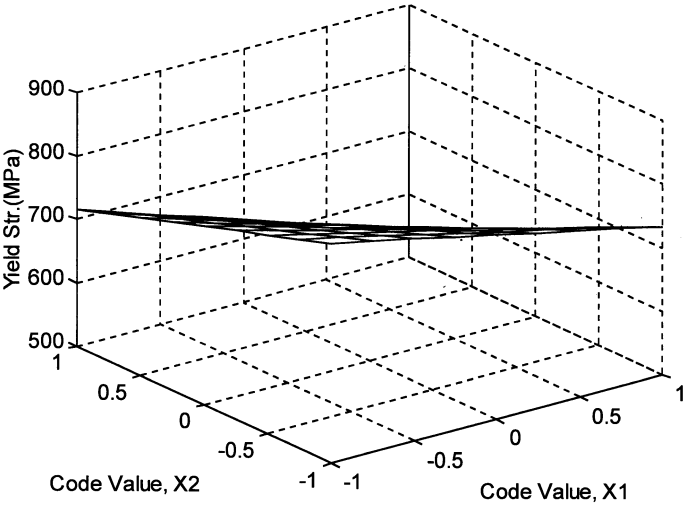

Fig. 14. Yield strength response surface (region: 600–700 °C and 0.33–2 h).

Table 5
Design matrix of heat treatment variables and responses (region: 600–700 °C and 0.33–2 h)

Heat treatment variables				Responses	
Tempering temperature		Tempering time		YS (MPa)	−50°C CVN value (J)
Coded value	Decoded value	Coded value	Decoded value		
X_1	x_1 (°C)	X_2	x_2 (h)		
−1	600	−1	0.33	846.6	135
−1	600	+1	2.00	716.1	196
+1	700	−1	0.33	733.8	258
+1	700	+1	2.00	544.5	232

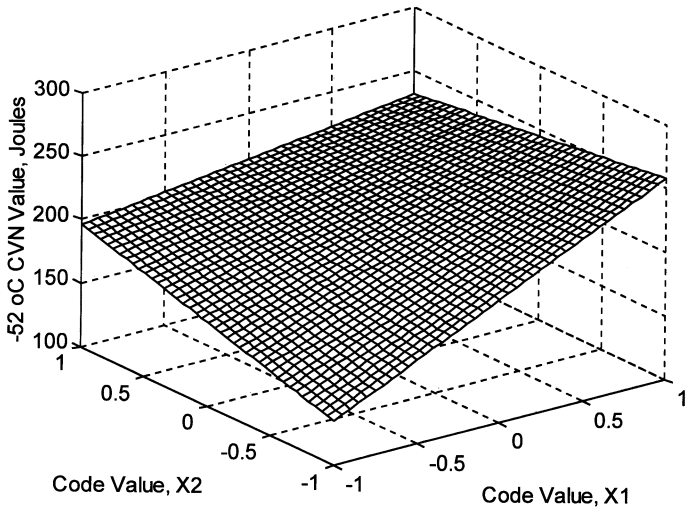

Fig. 15. Charpy response surface (region: 600–700 °C and 0.33–2 h).

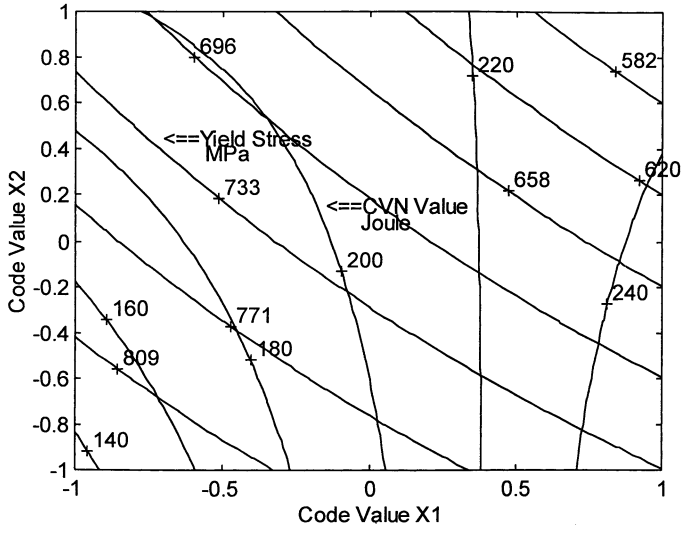

Fig. 16. Superimposed contour plot of YS and −50 °C CVN value (region: 600–700 °C and 0.33–2 h).

15). Using Eqs. (4) and (5) a nomogram is constructed (Fig. 16). These figures again point to the fact that the optimum combination of properties prevails at a tempering temperature above the base level value (> 650 °C) and a tempering time below the base level value (< 1.165 h). The nomogram is also useful in determining the heat treatment parameters (time and temperature of tempering) for any desired combination of properties (responses).

Use is made of this nomogram to get the starting point for the Steepest Ascent method. The iterations are carried out starting with the point $X_1 = 0.8$ and $X_2 = -0.8$. The third iteration gives the highest Charpy value of 256.53 J at $X_1 = -0.998$ and $X_2 = 0.896$ as shown in Table 6. Decoding the coded values using Eq. (6), the natural values of tempering temperature and time are obtained as 699.9 °C and 0.417 h, respectively. The YS calculated from Eq. (4) at this condition is 732.3 MPa.

For the purpose of optimization, Grid Search Technique was used and a suitable computer program was developed using FORTRAN language. The computer program utilized the regression Eqs. (4) and (5). The program searched for the condition where the Charpy value is maximum with a constraint of YS ≥ 730 MPa. The program calculates the Charpy value and the YS at different coded values of tempering temperature and time. Table 7 shows some of the results obtained from the computer. It is seen that the optimum condition occurs at $X_1 = 0.35$ and $X_2 = -0.55$. Decoding the above values using Eq. (6), it is found that the optimum combination occurs at a tempering temperature of 670 °C and a time of 0.5 h.

5. Conclusions

(1) Tempering the steel at 600 °C for different lengths of time shows discontinuous yielding. However, continuous yielding is observed for specimens tempered at 700 °C. This is a typical characteristic of Dual Phase steel. The same conclusion is also drawn from the plots of YS and TS against Hollomon–Jaffe parameter. The new austenite formed at higher tempering temperature transforms into martensite/bainite on quenching thus making a dual phase structure.

(2) The plot of ratio of YS/TS, calculated using the regression equations, shows that the ratio of YS to TS remains fairly constant below a tempering temperature of 615 °C. However, variation of ratio of YS to TS above 645 °C suggests formation of dual phase structure.

(3) The properties (YS, TS, −50 °C CVN value) are quantified with respect to time and temperature of tempering using classical curve fitting technique. The equations are valid within the experimental range of the variables (tempering temperature = 600–700 °C; tempering time = 0.33–12 h) and can be used to find out the properties at any combination of time and temperature of tempering within the experimental range.

(4) Plots are made for YS and Charpy values in a 3-dimensional space to help perceive the variation of the responses with the heat treatment process parameters. Superimposition of these plots reveals the feasible region of optimum combination of properties.

(5) Regression equations are developed over a smaller range of temperature and time of tempering (tempering temperature = 600–700 °C; tempering time = 0.33–2 h) using statistical design of experiments. A nomogram is constructed using these regression equations to give flexibility to the user in selecting the heat treatment process parameters to achieve any desired combination of properties.

Table 6
Iterative process of steepest ascent method

	Starting point	First iteration	Second iteration	Third iteration
X_1 (x_1)	0.8 (690 °C)	0.869 (693.45 °C)	0.937 (696.85 °C)	0.998 (699.9 °C)
X_2 (x_2)	−0.8 (0.497 h)	−0.832 (0.470 h)	−0.865 (0.443 h)	−0.896 (0.417 h)
−50 °C CVN value (J)	243.97	248.24	252.56	256.53

Table 7
Computer output of grid search technique

0.0500	2250.0000	
0.3000	−0.6000	
0.25000	−0.65000	
213.03438	746.82123	
0.25000	−0.60000	
213.20000	742.63995	
0.25000	−0.55000	
213.36563	738.45868	
0.30000	−0.65000	
215.72876	743.74402	
0.30000	−0.60000	
215.84000	739.52600	
0.30000	−0.55000	
215.95125	735.30792	
0.35000	−0.65000	
218.42313	740.66675	
0.35000	−0.60000	
218.48001	736.41193	
0.35000	−0.55000	
218.53688	732.15723	
The final values are		
218.53688	0.35000	−0.55000
732.15723		

(6) Maximization of property has been done by the method of Steepest Ascent. It is found that within the experimental range of variables a Charpy value of 256.5 J (at −50 °C) is obtainable at a tempering temperature of 700 °C and tempering time of 0.42 h.

(7) Optimization of the properties has been done by Grid Search technique. For this purpose a FORTRAN program was developed which can be used to find the maximum value of a property with a constraint on the other property.

(8) By proper selection of heat treatment parameters high strength together with high low-temperature toughness property can be achieved in copper precipitation strengthened HSLA-100 steel.

Acknowledgements

The authors would like to acknowledge the financial support provided by the U.S. Naval Research Laboratory through Directorate of Science and Technology (DST), India for carrying out this research project. The authors further acknowledge the coordination work done by the National Metallurgical Laboratory (CSIR), Jamshedpur, India.

References

[1] A.P. Coldren, T.B. Cox, Technical Report, David Taylor Research Laboratory, DTNSRDCN00167-85-C-006, 1985.
[2] E.J. Czyryca, Proc. Conf. on Advances in Low Carbon High Strength Ferrous Steels LCFA-92, O.N. Mohanty, B.B. Rath, M.A. Imam, C.S. Sivaramakrishnan (Eds.), Indo-US Pacific Rim Workshop, Trans Tech Pub., Jamshedpur, India, March 25–28, 1992, p. 490.
[3] A.D. Wilson, E.G. Hamburg, D.J. Colvin, S.W. Thompson, G. Krauss, Proc. of Conf. on Microalloyed HSLA Steels, ASM, Chicago, 1988, p. 259.
[4] S.J. Mikalac, M.G. Vassilaros, Proc. of Int. Conf. on Processing, Microstructure and Properties of Microalloyed and Other Modern High Strength Low Alloy Steels, Iron and Steel Society, Pittsburgh, PA, June 3–6, 1991, p. 331.
[5] M. Mujahid, A.K. Lis, C.I. Garcia, A.J. DeArdo, Proc. Conf. on Advances in Low Carbon High Strength Ferrous Steels LCFA-92, O.N. Mohanty, B.B. Rath, M.A. Imam and C.S. Sivaramakrishnan (Eds.), Indo-US Pacific Rim Workshop, Trans Tech Pub., Jamshedpur, India, March 25–28, 1992, p. 209.
[6] M. Mujahid, A.K. Lis, C.I. Garcia, A.J. DeArdo, Proc. Int. Conf. on Processing, Microstructure and Properties of Microalloyed and Other Modern High Strength Low Alloy Steels, Iron and Steel Society, Pittsburgh, PA, June 3–6, 1991, p. 345.
[7] Tither Geoffrey, Proc. Conf. on HSLA Steels Processing, Properties and Applications (October 28–November 2), TMS Pub, Beijing, China, 1990, p. 61.
[8] T.W. Montemarano, B.P. Sach, J.P. Gudas, M.G. Vassilaros, H.H. Vandervelt, J. Ship Prod. 2 (3) (1986) 145 (August).
[9] R.P. Foley, M.E. Fine, Proc. Int. Conf. on Processing, Microstructure and Properties of Microalloyed and Other Modern High Strength Low Alloy Steels, Pittsburgh, PA, Iron and Steel Society, June 3–6, 1991, p. 315.
[10] S.S. Rao, Optimization: Theory and Applications, Wiley Eastern, New Delhi, 1992. pp. 32–81, 301–309.
[11] R. Bronson, Theory and Problems of Operations Research, McGraw-Hill, Singapore, 1986, pp. 97–125.
[12] A.K. Panda, R.I. Ganguly, S. Misra, Tool Alloy Steels (1979) 101 (March/April).
[13] R.I. Ganguly, A.K. Panda, S. Misra, Trans. Iron Steel Inst. Jpn. 21 (1981) 577.
[14] W.G. Cochran, G.M. Cox, Experimental Design, Asia Publishing House, Mumbai, 1977, pp. 148–180.
[15] G.E. Dieter, Engineering Design, McGraw-Hill, Singapore, 1987, pp. 414–434.
[16] P.K. Ray, R.I. Ganguly, A.K. Panda, Influence of Heat Treatment Parameters on Structure and Mechanical Properties of an HSLA-100 Steel, Steel Research, Germany (in press).